

# A multiphysics and multiscale model for low frequency electromagnetic direct-chill casting

N Košnik<sup>1,2,4,a</sup>, A Z Guštin<sup>2b</sup>, B Mavrič<sup>2c</sup>, and B Šarler<sup>2,3,d</sup>

<sup>1</sup> Jožef Stefan Institute, Jamova 39, Ljubljana, Slovenia

<sup>2</sup> Institute of Metals and Technology, Lepi pot 11, Ljubljana, Slovenia

<sup>3</sup> University of Nova Gorica, Vipavska 13, Nova Gorica, Slovenia

<sup>4</sup> Department of Physics, University of Ljubljana, Jadranska 19, Ljubljana, Slovenia

E-mail: <sup>a</sup>nejc.kosnik@imt.si, <sup>b</sup>agnieszkazuzanna.gustin@imt.si, <sup>c</sup>bostjan.mavric@imt.si, <sup>d</sup>bozidar.sarler@imt.si

**Abstract.** Simulation and control of macrosegregation, deformation and grain size in low frequency electromagnetic (EM) direct-chill casting (LFEMC) is important for downstream processing. Respectively, a multiphysics and multiscale model is developed for solution of Lorentz force, temperature, velocity, concentration, deformation and grain structure of LFEMC processed aluminum alloys, with focus on axisymmetric billets. The mixture equations with lever rule, linearized phase diagram, and stationary thermoelastic solid phase are assumed, together with EM induction equation for the field imposed by the coil. Explicit diffuse approximate meshless solution procedure [1] is used for solving the EM field, and the explicit local radial basis function collocation method [2] is used for solving the coupled transport phenomena and thermomechanics fields. Pressure-velocity coupling is performed by the fractional step method [3]. The point automata method with modified KGT model is used to estimate the grain structure [4] in a post-processing mode. Thermal, mechanical, EM and grain structure outcomes of the model are demonstrated. A systematic study of the complicated influences of the process parameters can be investigated by the model, including intensity and frequency of the electromagnetic field. The meshless solution framework, with the implemented simplest physical models, will be further extended by including more sophisticated microsegregation and grain structure models, as well as a more realistic solid and solid-liquid phase rheology.

## 1. Introduction

Direct-Chill (DC) casting [5] turns out to be an efficient technology for production of aluminium semi-products. The process is robust and relatively simple, however it can induce a spectra of defects in the ingots. The control of the process, depending on the strand geometry and alloy composition, basically relies on adjusting the melt level, the casting speed, the melt temperature, and the intensity of the water jets that chill the ingot. These control parameters indirectly influence the melt flow and thus the solidification characteristics. An additional handle that can directly affect the flow is offered by alternating EM fields [6], applied to the DC process by means of coils placed around the casting system. The fields induce the eddy currents in the melt, which cause Lorentz force and thus provide a stirring force on the melt. A pioneering study of the application of low frequency electromagnetic field to the casting process was presented in [7], while a recent magnetohydrodynamic study of this problem was done by our group in [8]. The main aim of the present paper is the extension of this



model to include macrosegregation, mechanical effects and grain structure and thus forming a reasonably complete basic multiphysics and multiscale model of the process for the axisymmetric billets.

## 2. Macroscopic models

### 2.1. Thermofluid equations

We express all the governing macroscopic transport equations in cylindrical coordinates  $(r, z)$ , with base vectors  $\hat{\mathbf{e}}_r$  and  $\hat{\mathbf{e}}_z$  with  $z$  coordinate opposite to the casting direction. We limit ourselves to the cases where velocity vector points in the  $r-z$  plane. The mixture continuum concept [9], adjusted to DC casting with columnar only solid phase [10] is adopted. The momentum conservation equation accounts for the Darcy drag term, the volume force, which is decomposed into thermal and solutal Boussinesq buoyancy term and the Lorentz force term

$$\rho_m \frac{\partial}{\partial t}(\mathbf{v}_m) + \rho_m \nabla \cdot (\mathbf{v}_m \mathbf{v}_m) = -\nabla P_l + \nabla \cdot \left( \mu_l \frac{\rho_m}{\rho_l} \nabla \mathbf{v}_m \right) - \frac{\mu_l}{K} \frac{\rho_m}{\rho_l} (\mathbf{v}_m - \mathbf{v}_{\text{cast}}) + \mathbf{b}, \quad (1)$$

$$\mathbf{b} = -\rho_l \left[ \beta_{T,l} (T - T_0) + \sum_{i=1}^n \beta_{C,i} (C_l^i - C_0^i) \right] \mathbf{g} + \langle \mathbf{b}_{\text{EM}} \rangle. \quad (2)$$

The latter is denoted by  $\langle \mathbf{b}_{\text{EM}} \rangle$  and will be detailed in the following section. The solid phase velocity  $\mathbf{v}_s$  is assumed to be constant and equal to the casting velocity  $\mathbf{v}_s = \mathbf{v}_{\text{cast}}$ , that is parallel to the  $z$  coordinate. The mixture density and mixture velocity are defined as  $\rho_m = f_l \rho_l + f_s \rho_s$ ,  $\mathbf{v}_m = (f_l \rho_l \mathbf{v}_l + f_s \rho_s \mathbf{v}_s) / \rho_m$ , with  $f_l$  and  $f_s$  standing for the volume fraction of the liquid and solid phase, respectively. Mass conservation thus reads  $\nabla \cdot \mathbf{v}_m = 0$ . The permeability constant of the Darcy term, relevant in the mushy zone is modelled as  $K = K_0 f_L^3 (1 - f_L)^{-2}$ , and is set to 0 below the consolidation temperature, corresponding to  $f_l^{\text{lim}}$ , at which the liquid phase becomes trapped within the dendrites. The heat and species transfer is formulated with the mixture convection-diffusion equations

$$\frac{\partial}{\partial t}(\rho_m h_m) + \nabla \cdot (\rho_m h_m \mathbf{v}_m) = \nabla \cdot (\lambda_m \nabla T) - \nabla \cdot [\rho_m (h_l - h_m) (\mathbf{v}_m - \mathbf{v}_{\text{cast}})], \quad (3)$$

$$\begin{aligned} \frac{\partial}{\partial t}(\rho_m C_m^i) + \nabla \cdot (\rho_m C_m^i \mathbf{v}_m) = \\ = \nabla \cdot (\rho_m f_l D_l^i \nabla C_m^i) + \nabla \cdot [\rho_m f_l D_l^i \nabla (C_l^i - C_m^i)] - \nabla \cdot [\rho_m (C_l^i - C_m^i) (\mathbf{v}_m - \mathbf{v}_{\text{cast}})]. \end{aligned} \quad (4)$$

The enthalpy of the mixture is defined as  $h_m = f_l h_l + f_s h_s$ , where the constitutive relations are given as  $h_s(T) = \rho_s c_{ps} T$  and  $h_l(T) = \rho_l [c_{ps} T + c_{pl}(T - T_{\text{sol}})] + h_M$ , with  $h_M$  denoting melting enthalpy. We assume that  $f_l$  rises consistent with the Lever rule in the mushy zone,  $T > T_{\text{liq}}(C_m^i): f_l = 1, C_l^i = C_m^i$ ;  $T_{\text{liq}}(C_m^i) \geq T \geq T_{\text{sol}}(C_m^i): C_m^i = (1 - f_l) k^i C_l^i, T = T_{\text{liq}}(C_l^i)$ ;  $T < T_{\text{sol}}(C_m^i): f_l = 0, C_l^i = C_m^i / k^i$  and that the heat transfer coefficient is a weighted average of the phase coefficients  $\lambda = f_l \lambda_l + f_s \lambda_s$ . On the inlet boundary (north) of the axisymmetric domain we impose the fully developed Poiseuille flow profile with known casting temperature and nominal concentration of the alloying elements  $C_0^i$

$$\mathbf{v}_S = \mathbf{v}_L = -\hat{\mathbf{e}}_z v_{cast} \frac{2R^2}{R_{inlet}^2} \left( 1 - \frac{r^2}{R_{inlet}^2} \right), \quad T = T_{cast}, \quad (5)$$

where  $R_{inlet}$  and  $R$  are the inlet and mould radii, respectively. On the top free surface we set the temperature to the casting temperature and concentration to the nominal alloy concentration, and for the velocity, we set  $\partial v_r / \partial z = 0$ ,  $v_z = 0$ . On the left (symmetry) boundary, we prescribe  $v_r = 0$ ,  $\partial v_z / \partial r = 0$ ,  $\partial T / \partial r = 0$ ,  $C_l^i = C_0^i$ . On the right boundary (cooling side), the sticking boundary condition in the moving system is  $\mathbf{v} = -v_{cast} \hat{\mathbf{e}}_z$ . The cooling side temperature boundary condition is modelled with the Robin boundary condition  $-k \partial T / \partial r = h(z)(T - T_{env})$ , where  $h(z)$  takes into account variation of the heat transfer coefficient with coordinate  $z$ . It vanishes in the hot-top region. In the mould chill region we set it to a constant value  $h_{MC}$  whereas in the direct chill region it starts at value  $h_{DC}$  just below the mould chill and linearly rises to  $3h_{DC}$  on the bottom of the direct chill region. Finally, on the bottom boundary we require constant field derivatives in the casting direction  $\partial T / \partial z = 0$ ,  $\partial v_z / \partial z = 0$ ,  $v_r = 0$ ,  $\partial C_l^i / \partial z = 0$ .

### 2.2. Electromagnetic field equations

The dynamical pair of Maxwell equation is

$$\nabla \times \mathbf{E} = -\frac{\partial \mathbf{B}}{\partial t}, \quad \nabla \times \mathbf{B} = \mu_0 \mathbf{J} + \frac{1}{c^2} \frac{\partial \mathbf{E}}{\partial t}, \quad (\mu_0 = 4\pi \times 10^{-7} \text{ Vs / Am}), \quad (6)$$

where we assume  $c = \infty$  and work in the quasi-static approximation. Electric ( $\mathbf{E}$ ) and magnetic ( $\mathbf{B}$ ) fields are both divergence-free, i.e., solenoidal. In addition, the Ohm's law in the moving frame relates fields with induced eddy currents,  $\mathbf{J} = \sigma(\mathbf{E} + \mathbf{v} \times \mathbf{B}) + \mathbf{J}_{ext}$ , where  $\sigma$  is conductivity that is nonzero only in the conductor, whereas  $\mathbf{J}_{ext}$  is nonzero only in the coil and can be viewed as a boundary condition. We work with the electromagnetic potential  $\mathbf{A}$  defined through  $\mathbf{E} = -\nabla \phi - \frac{\partial \mathbf{A}}{\partial t}$ ,  $\mathbf{B} = \nabla \times \mathbf{A}$  and impose the Coulomb gauge,  $\nabla \cdot \mathbf{A} = 0$ , for the vector potential.

Maxwell equations thus reduce to the induction equation for  $\mathbf{A}$

$$\nabla^2 \mathbf{A} = \mu_0 \sigma \left( \frac{\partial \mathbf{A}}{\partial t} - \mathbf{v} \times \nabla \times \mathbf{A} \right) - \mu_0 \mathbf{J}_{ext}, \quad \phi = 0. \quad (7)$$

We set  $\mathbf{v} = \mathbf{0}$  on the right-hand side since the effect of velocity on the EM field is small in regime of small magnetic Reynolds number. Details of the equations in axisymmetry are given in [8].

### 2.3. Solid mechanics equations

The solid mechanics model is solved by assuming the calculated temperature field from the thermal model. The assumed thermoelastic governing equation is

$$G \nabla^2 \mathbf{u} + (G + \lambda) \nabla \nabla \cdot \mathbf{u} + \nabla \lambda \nabla \cdot \mathbf{u} + \nabla G [\nabla \mathbf{u} + (\nabla \mathbf{u})^T] = \nabla [\beta_T (T - T_{ref})] - \mathbf{f}, \quad (8)$$

where  $G$  stands for shear modulus,  $\lambda$  for Lamé parameter and  $\mathbf{f}$  is the body force. The coupling with the temperature field is described by the coefficient  $\beta$  defined as  $\beta = (3\lambda + 2G)\alpha$  which is composition dependent. Another free parameter is the reference temperature  $T_{ref}$ , which denotes the temperature at which the thermal expansion is considered to be zero.

## 3. Microscopic models

The microscopic model is solved in a post-processing mode. The model inputs temperature and concentration data from the macroscopic model. The representative input data are taken from the billet center, middle and surface streamlines in Lagrangean sense. The time for microscopic model is calculated from the velocity and length of the streamline. A typical 3x3mm representative traveling area is considered on each of the three considered streamlines.

### 3.1. Nucleation kinetics

To describe the nucleation event the continuous log normal nucleation model is adopted. The variation of the grain distribution in each time step depends on the undercooling temperature in the bulk of the casting. The density of grains  $n(\Delta T_{nuc})$  activated at the given degree of undercooling  $\Delta T_{nuc}$  is given by the integral of nucleation density distribution

$$\frac{dn}{d\Delta T_{nuc}} = \frac{n_{max}}{\sqrt{2\pi}\Delta T_{\sigma}} \frac{1}{\Delta T_{nuc}} \exp\left[-\frac{1}{2}\left(\frac{\ln \Delta T_{nuc} - \ln \Delta T_0}{\Delta T_{\sigma}}\right)^2\right], \quad (9)$$

where  $\Delta T_0, \Delta T_{\sigma}, n_{max}$  represent the mean nucleation undercooling, the standard deviation and the maximum density of nuclei that can form in the melt, respectively. These three standard nucleation parameters are determined experimentally for each alloy and grain refiner by measuring the grain size.

### 3.2. Grain growth kinetics

A modified KGT model is used to predict the grain growth velocities. The growth process is driven [11] by the local undercooling, approximated from the linearized phase diagram of a multicomponent

alloy  $\Delta T = T_{liq} - T(t) + \sum_{i=1}^n m_i (C_i^l - C_0^i)$ , where  $T_{liq}, T, m_i, C_0^i, C_i^l$  represent the liquidus temperature, the temperature recalculated from the macroscopic model, the liquidus slope of species  $i$ , the initial concentration of species  $i$  and the liquid concentration of species  $i$ , recalculated from the macroscopic model. In order to calculate the grain velocity  $V$ , the transport equations are solved for each species  $i$ .

The solution relates the nondimensional supersaturations for each alloying element  $i$ , to the corresponding growth Péclet number  $\Omega_i = F(P_i)$ ,  $P_i = rV / 2D_i^l$  where  $r$  is a tip radius. The supersaturation  $\Omega_i$  is expressed by the Ivantsov function for the purely diffusive growth regime  $F(P_i) = P_i \exp(P_i) E_1(P_i)$  where  $E_1$  is the integral exponential function. The total undercooling can be expressed as

$$\Delta T = \sum_{i=1}^n m_i C_0^i \left(1 - \frac{1}{1 - (1 - k_i) F(P_i)}\right), \quad (10)$$

where  $m_i$  is the liquidus slope of species  $i$ . The marginally stable plane front solution is applied in order to select the solution  $V(\Delta T)$ , with  $r = \frac{1}{\sqrt{V}} \sqrt{4\pi^2 \Gamma / \sum_{i=1}^n m_i (k_i - 1) C_i^l / D_i^l}$ , and  $\Gamma$  standing for the Gibbs-Thomson coefficient.

## 4. Solution procedures

The time-averaged Lorentz force is calculated by discretizing the computational domain in local domains with 9 nodes with the approximation function expressed as a minimum least squares fit of 6 monomials  $(1, x, y, xy, x^2, y^2)$ . The weight function in the least squares problem is chosen to be

Gaussian,  $e^{-r^2/\xi}$ .  $\xi$  is an average squared distance from the center node to all nodes in the local domain. The sparse linear system is solved using the sparse system solver [12]. The EM field calculation domain extends  $1.5H$  beyond the casting system in vertical direction and is terminated at  $3R$  in the radial direction (see figure 2). Unstructured node arrangement is used for the EM field calculation that has embedded the nodes for the thermofluid equations in a way that in the mould the EM and thermofluid nodes coincide. The transport equations for mass, momentum, energy, and concentration are solved by collocation with multiquadrics radial basis functions with 5-noded subdomains in case of the thermal model (as described in [13, 14]) and 6-noded subdomains in case of the mechanical model as elaborated in the present proceedings [15]. The phase change kinetics equations are solved by the PA method. The representative microscopic calculation domain with a dimension  $3 \times 3$  mm is discretized into 360 000 randomly located nodes. The post processing calculations of temperature and concentration for this domain are taken from the macro level of calculations. The details of the PA method are elaborated in [16]. The potential nucleation grains are randomly located in this domain in each time step. The new grain represents a new family and gets a randomly chosen orientation (color) at the time when it appears. As grains nucleate, they start to grow with respect to the PA neighborhood configuration which is associated with the position of the neighboring PA nodes which fall into a circle with assumed radius  $R_h = 0.5 \mu\text{m}$ . Due to the random arrangement of the nodes the neighborhoods are different. For the given values of the physical and thermodynamic properties  $m_i, k_i, D_i^i$  of each alloy element  $i$ , the variable grain growth velocity  $V$  for a specified undercooling temperature  $\Delta T$  can be calculated. Independent calculations of the growth velocity for a given set of these values are carried out in each time step by using an iterative method. This requires the micro model to be provided with values of  $T$  and  $C_i^i$ , taken from the macro model at every 0.05 s.

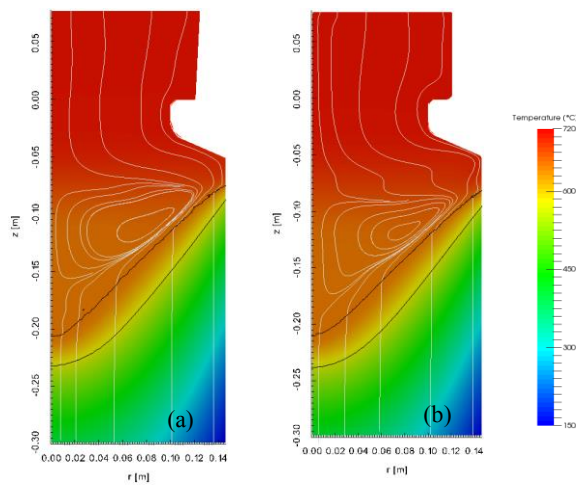


**Figure 1.** Temperature and velocity profiles for casting speed 80 mm/min without (a) and with (b)  $I=10\text{A}$ ,  $f=10\text{Hz}$  EM field.

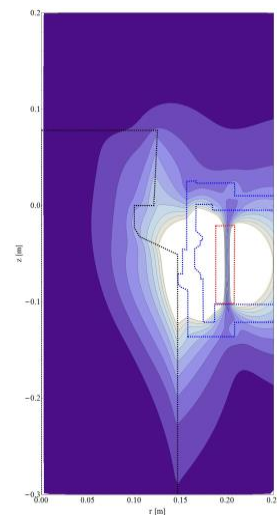


**Figure 2.** Computed magnitude of the magnetic field  $I=10\text{A}$ ,  $f=10\text{Hz}$ .

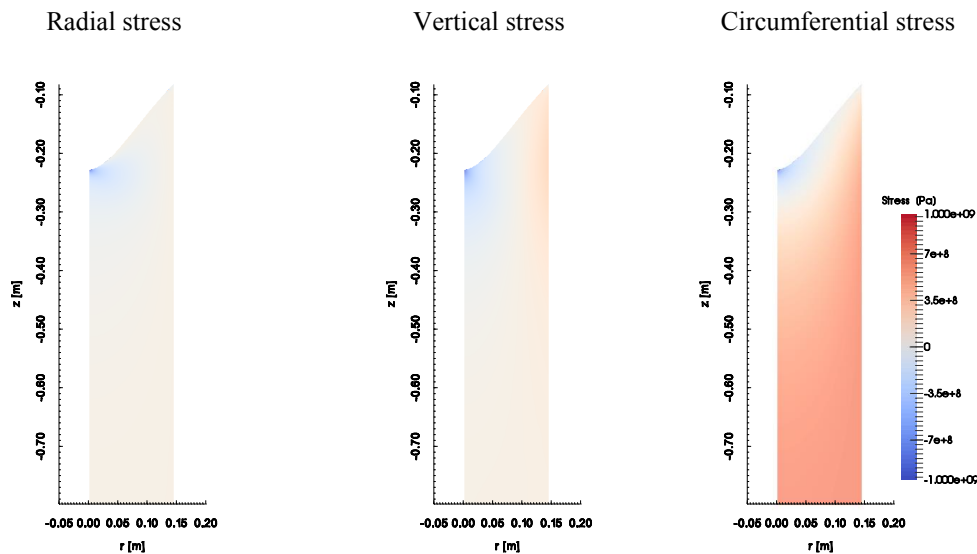


**Figure 3.** Stress calculations from the thermoelastic model at conditions from figure 1 (a).

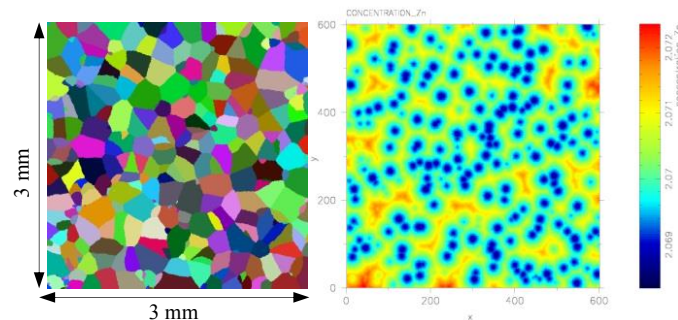


**Figure 4.** Results from the grain structure model. Left: grain structure. Right: Zn concentration for Al- Zn-5.3% Mg-2.35% Cr-1.5% Cu-0.5% alloy at conditions from figure 1(a).

## 5. Implementation of the models

The capabilities of the model are demonstrated in figures 1- 4 at various process parameters. Figure 1 shows the temperature field without and with EM field. Figure 2 shows computed magnitude of the magnetic field. Figure 3 shows stress calculations from the thermoelastic model for radial, vertical and circumferential stress. Figure 4 presents grain structures and Zn concentration distribution.

## 6. Conclusions

A reasonably complete multiphysics and multiscale model of the low frequency electromagnetic casting has been developed. The electromagnetic field is calculated first, afterwards the momentum equation, pressure velocity-coupling, energy equation, and species equations. The mechanical calculations are performed without feedback, based on the thermal calculations. The microstructure calculations are coupled in Lagrangean sense to the calculated velocity and concentration fields in a post-processing mode. The models are on the macro level solved by the diffuse approximate method and on the micro-level by the point automata method. This novel approach is completely meshless and no polygonisation is needed. The considered physical models incorporate only simple, basic elements that obviously need further improvements. In the field of macrosegregation, the movement of the solid phase and influence of the grain refiner represent the next necessary steps [17]. In the field of solid mechanics, the introduction of viscoelastic behaviour and feedback to the thermal model (mould heat

transfer) seems important. In the field of microstructure modelling, the inclusions of the secondary phases in the model are necessary. It should be pointed out that the extension of the present numerical approach to three dimensions seems straightforward, since the coding of the present axisymmetric meshless formulation is equivalent in higher dimensions.

### Acknowledgements

Support from the Slovenian Grant Agency in the framework of the project L2-6775 and IMPOL Aluminium Industry is kindly acknowledged.

### References

- [1] Vertnik R, Založnik M and Šarler B 2006 *Eng. Anal. Bound. Elem.* **30** 847-55
- [2] Šarler B and Vertnik R 2006 *Comput. Math. Appl.* **51** 1269-82
- [3] Chorin A J 1967 *J. Comput. Phys.* **2** 12-26
- [4] Lorbiecka A Z and Šarler B 2014 *Materials Science Forum* **790-791** 115-20
- [5] Eskin D G 2008 *Physical Metallurgy of Direct Chill Casting of Aluminium Alloys*, (Boca Raton: CRC Press/Taylor & Francis)
- [6] Davidson P A 2001 *An Introduction to Magnetohydrodynamics*, (Cambridge: Cambridge University Press)
- [7] Dong J and Cui J Z 2004 *Metall. Mater. Trans.* **35A** 2487-95
- [8] Košnik N, Vertnik R and Šarler B 2004 *Materials Science Forum* **790-791** 390-395
- [9] Bennon W D and Incropera F P 1988 *Numer. Heat Transf.* **13A** 277-96
- [10] Du Q, Eskin D G and Katgerman L 2007 *Metall. Mater. Trans.* **38A** 180-89
- [11] Appolaire B, Combeau H and Lesoult G 2007 *Mater. Sci. Eng. A* **487** 33-45
- [12] Schenk O and Gärtner K 2004 *Journal of Future Generation Computer Systems* **20** 475-487
- [13] Kosec G Založnik M, Šarler B and Combeau H 2011 *Comput. Mater. Cont.* **22** 169-59
- [14] Kosec G and Šarler B 2014 *Eng. Anal. Bound. Elem.* **45** 36-44
- [15] Mavrič B and Šarler B (in present proceedings)
- [16] Lorbiecka A Z and Šarler B 2010 *CMC* **18** 69-104
- [17] Nadella R, Eskin D G, Du Q and Katgerman L 2008 *Progress in Materials Science* **53** 421-480